AIAA/AAS Astrodynamics Specialist Conference and Exhibit
5-8 August 2002, Monterey, California

AIAA 2002-4643

3D MODELING OF AN ELASTIC TETHER USING A DISSIPATIVE TIME-STEPPING ALGORITHM

Michael D. Jokic*, William J.T. Daniel†,
The University of Queensland, St Lucia, QLD 4072, Australia
and
James M. Longuski‡
Purdue University, West Lafayette, IN 47907-1282, U.S.A.

A three-dimensional simulation of an aerobraking maneuver is investigated using a dissipative time-stepping algorithm. The system modelled consists of an atmospheric probe connected to an orbiter by a thin, elastic tether. A dissipative time-stepping scheme, developed from the generalised-alpha method, is used to accurately predict the highly nonlinear dynamics of the flexible system. The simulations include atmospheric and gravitational models corresponding to an oblate planetoid. A three-dimensional aerobraking maneuver is simulated for a tethered system orbiting Mars.

INTRODUCTION

Flexible systems have inherent modeling complexities that can result in unstable solutions to the equations of motion integrated with respect to time. An accumulation of momentum and energy is often evident in these systems, which ultimately results in poor model accuracy. The generalized-alpha method is one of several schemes that have been proposed to address this problem through dissipation of high-frequency vibrations. Developed from the Newmark method, the generalized-alpha method evaluates system forces at a fraction α_f of a cycle and the inertia terms at a fraction α_m. Kuhl and Crisfield[1] apply an implicit version of the scheme to problems involving finite deformations and finite rotations. In a recent paper, Daniel[2] outlines an explicit form of the generalized-alpha method that can mesh with the implicit form. It is an explicit variant that is implemented in the current research to propagate the highly nonlinear dynamics of a tethered system. Bauchau et al.[3] and Armero and Romero[4] present alternative approaches to the nonlinear dynamics of elastic systems. The robust scheme outlined by Bauchau et al.[3] is shown to be energy and momentum conserving in the nonlinear case but requires significant computation per time step.

The potential applications for tethered systems that interact with the atmosphere of a planet are numerous. Phenomena and properties of regions in Earth's upper atmosphere that can be investigated using a probe tethered to an orbiting mass.[5, 6] In addition, an aerothermodynamic testing facility,[7] an upper stage of a launch system,[8] and dust collection from the Martian atmosphere[9,10] using tethers have also been proposed. Complementing the breadth of concepts that relate to atmospheric applications of tethered systems is the research conducted into modeling this class of missions. No and Cochran[11, 12] and Bae et al.[13] develop dynamic models of flight vehicles tethered to orbiting masses. Consideration of the aerodynamic effects on a tethered system in the flow regimes in which the system operates is addressed in recent work.[14, 15]

Aeroassisted orbital maneuvering of tethered satellite systems is the focus of several research efforts. Longuski and Puig-Suari[16] successfully demonstrate the implementation of aerobraking and aerocapture maneuvers at Mars using a tethered satellite system with a dumbbell configuration. This work is extended to include locations throughout the solar system[17] and optimized to minimize the tether mass.[18] Biswell[19] develops a three-dimensional hinged-rod model of an

* Ph.D. Candidate, Department of Mechanical Engineering. Member AIAA.
† Lecturer, Department of Mechanical Engineering.
‡ Professor, School of Aeronautics and Astronautics, Associate Fellow AIAA, Member AAS.

Copyright © 2002 by Michael D. Jokic, William J.T. Daniel and James M. Longuski. Published by the American Institute of Aeronautics and Astronautics, Inc. with permission.

Copyright © 2002 by the author(s). Published by the American Institute of Aeronautics and Astronautics, Inc., with permission.

elastic tether to predict the behavior and performance of the aerocapture maneuver in detail. In addition, recent work demonstrates aerogravity assist maneuvering of a tethered satellite system[20] during a flyby of Mars.

This paper presents the implementation of an explicit time-stepping algorithm derived from the generalized-alpha method. Specifically, the algorithm is applied to tethered systems performing aeroassisted orbital maneuvers. The dissipative properties of the algorithm produce a stable simulation of aerobraking maneuvers. The simulations further demonstrate the propellant-free adjustment of a tether system using planetary atmospheres.

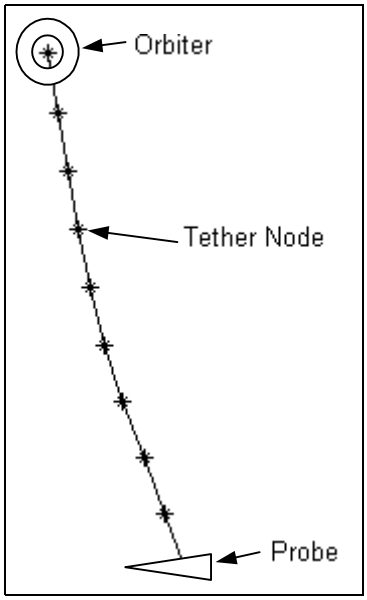

Figure 1: Elastic tethered system configuration.

SYSTEM MODELING

The system investigated consists of an atmospheric probe connected by a thin tether to a primary orbiting mass. For modeling purposes, the tether is discretized into a series of nodes. Figure 1 depicts a deformed tether after interaction with an atmosphere. The orbiter mass, m_o, and probe mass, m_p, are assumed to be concentrated at a point.

The mechanical properties of Spectra 2000 are used in the simulations of the elastic tethered systems. Table 1 outlines the relevant properties of this material.

Table 1: Tether material properties

Tether Tensile Strength	3.5 GPa
Tether Modulus of Elasticity	124 GPa
Tether Material Density	970 kg/m^3

The Dissipative Time-Stepping Algorithm

The time-stepping algorithm used in the current research is an explicit, predictor-multi-corrector algorithm. In each time step, this variant of the generalized-alpha method first predicts the new velocity and the change in displacement of a system element using

$$v_{n+1} = v_n + a_n \Delta t \left(\tfrac{1}{2} - \alpha_f\right) \big/ \left(1 - \alpha_m\right) \qquad (1)$$

$$u_{n+1} = u_n + v_n \Delta t \,. \qquad (2)$$

Here, α_f and α_m are the parameters of the generalized-alpha method. For the simulations of the aeroassisted orbital maneuvering of tethered systems, the forces are evaluated at the midpoint of a cycle (i.e. $\alpha_f = 0.5$). This has the advantage of conserving angular momentum in each cycle. During each time step, u_n is set to zero by updating the reference axes. The acceleration parameter, α_m, is defined as

$$\alpha_m = \left(2\rho_b - 1\right) \big/ \left(\rho_b + 1\right) \qquad (3)$$

where, ρ_b is the minimum spectral radius, which is a measure of the high-frequency numerical damping. A ρ_b value of 1 corresponds to no numerical damping and value of 0 to the maximum available to the algorithm.

The prediction of the new state values is corrected over multiple iterations using the Newmark equations, which are defined as

$$v_{n+1} = v_n + (1-\gamma) a_n \Delta t + \gamma a_{n+1} \Delta t \qquad (4a)$$

$$u_{n+1} = u_n + v_n \Delta t + \beta a_{n+1} \Delta t^2 + (\tfrac{1}{2} - \beta) a_n \Delta t^2 \qquad (4b)$$

To maintain the same eigenvalues of the amplification matrix and the same dissipative properties of the method presented by Chung and Hulbert,[22] gamma and beta are defined as

$$\gamma = 1 - \alpha_m \tag{5a}$$

$$\beta = (5 - 3\rho_b)(1 + \rho_b)^{-1}(2 - \rho_b)^{-1} - \gamma/2 \tag{5b}$$

The acceleration is updated by

$$a_{n+1} = \left(-F_{int} + F_{aero} + F_{grav}\right) M_{corr}^{-1} (1 - \alpha_m)^{-1} - \alpha_m (1 - \alpha_m)^{-1} \alpha_n^{-1} \tag{6}$$

where, F_{int}, F_{aero} and F_{grav} are the internal, aerodynamic and gravitational forces acting on the system, respectively. M_{corr} represents the effective system mass, which is corrected for damping due to aerodynamic forces and is defined as

$$M_{corr} = M + 2F_{aero} v_{wind}^{-1} (1 - \alpha_f)(1 - \alpha_m)^{-1} \gamma \Delta t \tag{7}$$

The predicted value is corrected until the error between the new prediction and the old prediction of the displacements reaches a desired value. The error, e, is determined using

$$e = (u_{n+1} - u_n)^2 u_n^{-2}. \tag{8}$$

The algorithm is second order accurate for ρ_b equal to 1 and has a minimum stability limit associated with ρ_b equal to 0 of

$$\Delta t_{\max} = \sqrt{2}\ \omega_{n\max}^{-1}. \tag{9}$$

The maximum time step shown in Eq. 9 is the worst case corresponding to the maximum possible numerical damping being present in the algorithm.

Internal Forces

The internal forces present in the tethered system are a function of the generalized mid-point Green strain. As presented by Kuhl and Crisfield[1], the internal forces can be calculated by

$$\mathbf{F}_{\text{int}} = (A_o E / l_o)\mathbf{A}(\mathbf{x}_{\alpha_f})\left[(1 - \alpha_f)\varepsilon(\mathbf{u}_{n+1}) + \alpha_f \varepsilon(\mathbf{u}_n)\right] \tag{10}$$

where, $\varepsilon(\mathbf{u})$ represents the modified Green strain, which is a function of the displacements of an element's end points. $\boldsymbol{x}_{\alpha f}$ is a vector containing the coordinates of the end points of a tether element at a fraction α_f of a cycle relative to a reference position, and the vector $\mathbf{u}$ contains the displacements of the end points. The terms A_o, l_o and E represent the undeformed cross-sectional area of the element, the undeformed length and elastic modulus of the material, respectively. As mentioned previously, α_f is specified to be 0.5 to evaluate the forces at the mid-point of a cycle. $\mathbf{A}$ is a matrix of third-order identity matrices and is defined as

$$\mathbf{A} = \begin{pmatrix} I_3 & -I_3 \\ -I_3 & I_3 \end{pmatrix}. \tag{11}$$

Gravitational Forces

We adopt a non-spherically symmetric gravitational field model for determining the gravitational forces. Ignoring terms that are longitudinally dependent, the gravitational potential takes the form[23]

$$V = -\mu/r\left[1 - \sum_{k=2}^{\infty} (R/r)^k J_k P_k \cos\phi\right], \tag{12}$$

where μ is the gravitational constant for the planet, R is the radius of the planet, J_k are constant coefficients, ϕ is the colatitude and P_k are the Legendre polynomial functions. The gravitational potential is determined for terms with k equal to two.

An algorithm that estimates the equations of motion at the midpoint of a cycle will conserve energy for a force associated with a potential[21], V, if the estimate of the force is

$$\mathbf{F}_{n+½} = (V_{n+1} - V_n)(R_{n+1} - R_n)^{-1} \mathbf{R}_{n+½} / R_{n+½} \tag{13}$$

where $\mathbf{F}_{n+½}$ is the force evaluated at the midpoint of a cycle. $\mathbf{R}_{n+½}$ represents the vector from the center of the planet to the center of the object at the midpoint of a cycle and $R_{n+½}$ is the corresponding magnitude.

Aerodynamic Forces

The atmosphere is assumed to rotate with the planet at an angular velocity Ω for calculating the aerodynamic forces. In addition, an exponential model for the density distribution in the atmosphere is adopted. For a body at radius R_k, the density is determined by

$$\rho_k = \rho_{ref} \exp\left[\left(H_r - R_k + R_{pl}\right)/H\right]. \tag{14}$$

In this equation ρ_{ref} is the reference atmospheric density, H_r represents the model reference height, H is the scale height and R_{pl} is the radial distance to the

surface of the planet. The planetoid is treated as an ellipsoid described by

$$x = R_{eq} \cos\theta \sin\phi \qquad 15(a)$$

$$y = R_{eq} \sin\theta \sin\phi \qquad 15(b)$$

$$z = R_{pole} \cos\phi, \qquad 15(c)$$

where, R_{eq} is the equatorial radius of the planet, R_{pole} is the polar radius, θ is the longitude of the planet and ϕ is the colatitude. x, y and z represent the Cartesian components of R_{pl} The aerodynamic forces are calculated when the system is within 300 km of the surface of Mars. For the aerodynamic force calculations, the radial distance of a mass at the midpoint of a cycle is used.

Aerodynamic Drag

The aerodynamic drag acting on the orbiter, tether and probe is assumed to follow

$$\mathbf{F} = -\tfrac{1}{2} \rho C_d S V \mathbf{V}, \qquad (16)$$

where C_d is the drag coefficient, S is the frontal area of the body and $\mathbf{V}$ is the velocity relative to the atmosphere. The drag force acting on the orbiter is

$$\mathbf{F}_{do} = -\tfrac{1}{2} \rho_o C_{do} S_o V_o \mathbf{V}_o, \qquad (17)$$

where C_{do}, S_o , ρ_o and V_o represent the drag coefficient, frontal area, atmospheric density and relative velocity corresponding to the orbiter, respectively.

For the aerobraking scenario, the atmospheric probe is assumed to be a sphere. The aerodynamic drag calculation, therefore, is of the same form as the orbiter. With the appropriate subscript substitution, the drag on the probe during an aerobraking maneuver is calculated using

$$\mathbf{F}_{dp} = -\tfrac{1}{2} \rho_p C_{dp} S_p V_p \mathbf{V}_p. \qquad (18)$$

To determine the aerodynamic drag acting on the tether the frontal area of the tether is lumped to the nodes. The aerodynamic drag is calculated for each lumped area using the atmospheric density and relative velocity at the node. The drag force acting at the ith node can be represented as

$$\mathbf{F}_{di} = -\tfrac{1}{2} \rho_i C_{dt} S_i V_i \mathbf{V}_i, \qquad (19)$$

where, C_{dt} denotes the drag coefficient of the tether and S_i represents the tether frontal area lumped at the node.

NUMERICAL RESULTS

Two sets of results are presented here for the numerical simulations of elastic tether systems. It is important to note that no attempt has been made to incorporate the mission elements identified by Longuski et al.[17] to improve the dynamic response of the system. In this way, it is possible to test the ability of the simulation model to accommodate non-ideal mission scenarios.

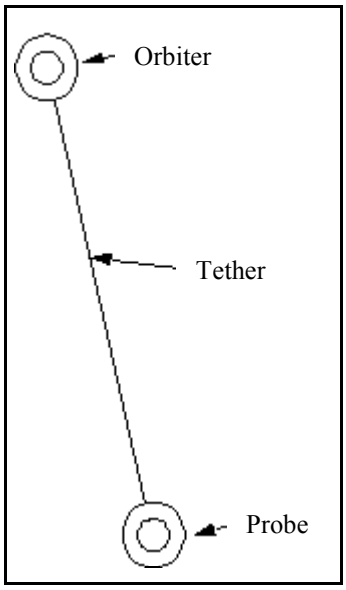

Figure 3: Single-link tethered system

Algorithm Comparison

To test the performance of the modified generalized-alpha method presented in this paper, a benchmark problem is modeled. The scenario adopted for the comparison consists of an orbiter and a probe connected by a single-link, massless, elastic tether. This system is put into an elliptic orbit about Mars with the assumption that there are no atmospheric forces acting. Figure 3 depicts the configuration of the tether system used for the algorithm comparison. The orbit properties and the physical properties of the system are presented in Table 2 and Table 3, respectively.

The single-link configuration is easily implemented using the mid-point modification of the generalized-alpha method. For comparison, the equations of motion for a system consisting of two masses connected by a simple spring have been derived using Lagrange's equation, which is defined as

$$\frac{d}{dt}\frac{\partial L}{\partial \dot{q}} - \frac{\partial L}{\partial q} = 0. \qquad (20)$$

The resulting nonlinear equations of motion are propagated in time using an explicit Runga-Kutta numerical solver in MATLAB.

Table 2: Initial orbit properties for the benchmark scenario

Periapse Altitude	180 km
Eccentricity of Initial Orbit	0.5
Mars Radius	3397 km

Table 3: Physical properties of the tether system for the benchmark scenario

Orbiter Mass, m_o	1000 kg
Probe Mass, m_p	1000 kg
Tether Length	150 km
Tether Diameter	5 mm

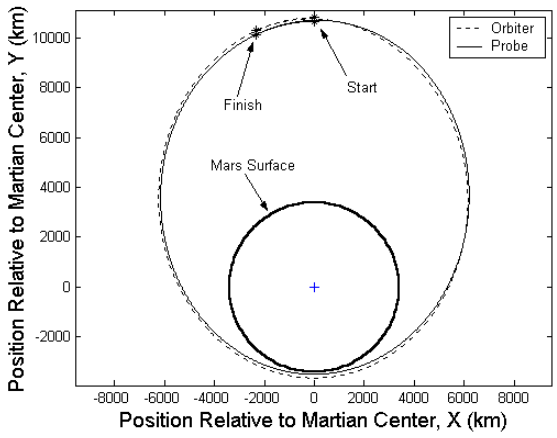

Figure 4: System orbit propagated using the dissipative time-stepping algorithm.

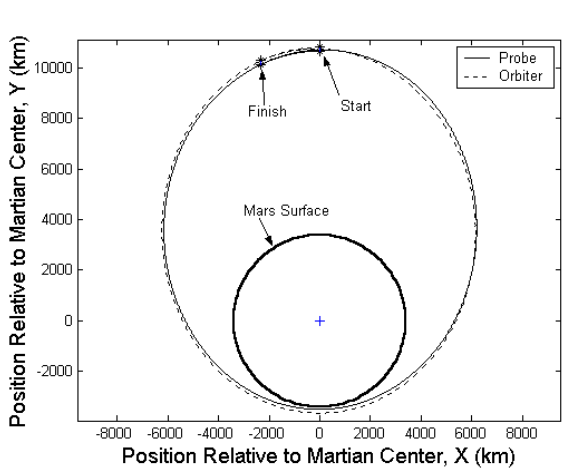

Figure 5: System orbit propagated using a Runga-Kutta numerical solver.

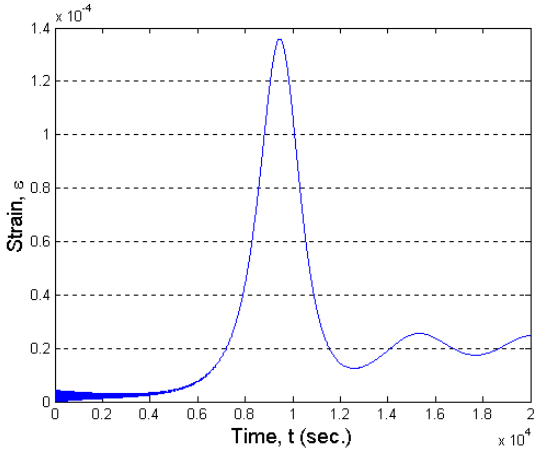

Figure 6: Strain history using the dissipative time-stepping algorithm.

Figure 4 and Fig. 5 show the trajectories of the orbiter and probe for the dissipative algorithm and the MATLAB numerical solver, respectively. At this level, there is no discernable difference between the two results. In both simulations, the tether system spins at the same rate with the orbiter and probe trajectories crossing at the same positions. Figure 6 displays the strain history of the tether for the simulation using the dissipative time-stepping algorithm. As can be seen in the figure, a stable response is produced with some high frequency vibration during the first stages of the orbit due to the initial conditions.

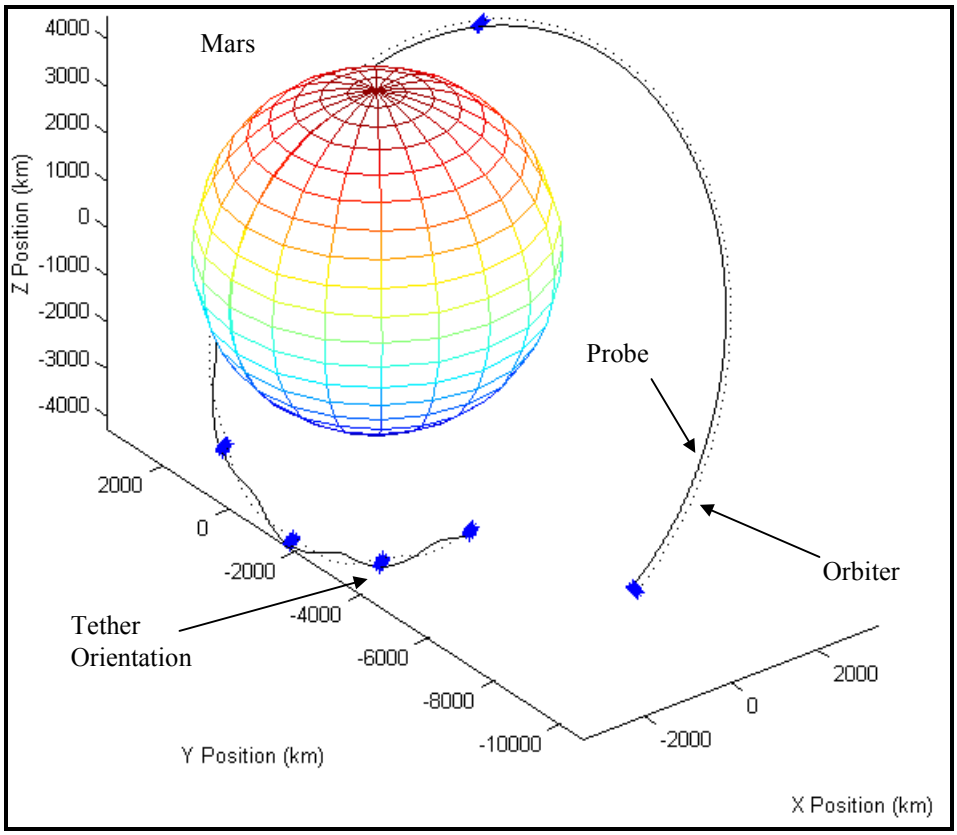

Figure 7: Trajectory of a tethered system during an aerobraking maneuver.

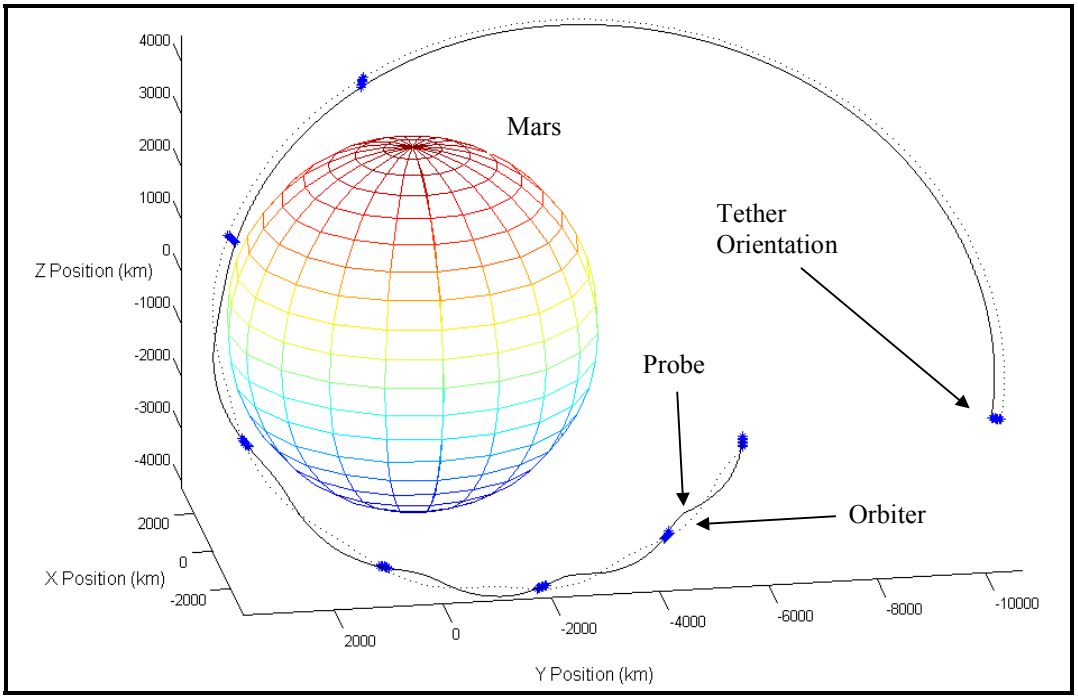

Figure 8: Trajectory of a tethered system during an aerobraking maneuver.

Aerobraking Maneuver

A representative aerobraking maneuver is simulated for an uncontrolled elastic tethered system using the dissipative time-stepping algorithm. Table 4 contains the physical properties for the tether system in the simulation. In this scenario, the tether is discretized into six segments. The probe and orbiter are idealized as spheres for the purpose of determining the aerodynamic forces. Table 5 shows the characteristics of the arbitrary initial orbit. The simulation commences at apoapse and terminates 3.88 hrs (flight time) later. The numerical damping in the algorithm (spectral radius) is set to 0.9.

Table 4: Physical properties of the tether system for the aerobraking scenario

Orbiter Mass	1000 kg
Probe Mass	500 kg
Tether Length	180 km
Tether Diameter	2 mm
Orbiter Drag Coefficient	2
Tether Drag Coefficient	2
Probe Drag Coefficient	1
Probe - Frontal Surface Area	1 m^2
Number of Tether Segments	6

Table 5: Initial orbit properties for the aerobraking scenario

Periapse Altitude	200km
Eccentricity of Initial Orbit	0.5
Mars Radius	3397 km
Assumed Mars Atmosphere Altitude Limit	300 km

The effect of the interaction between the system and the atmosphere of Mars on the initial orbit can be clearly seen in Figs. 7 and 8. After penetrating the atmosphere, the apoapse of the tethered system's orbit is lower than its initial altitude and the system begins rotating. Figures 7 and 8 clearly show the ability of the modeling technique to represent the three-dimensional behavior of a tethered system undergoing orbital maneuvers.

Strain information for each of the tether links is used to update the internal forces and the location of the tether nodes. This information is recorded as the tether system is propagated in time. Figures 9 and 10 represent the strain history of the links attached to the probe and orbiter, respectively.

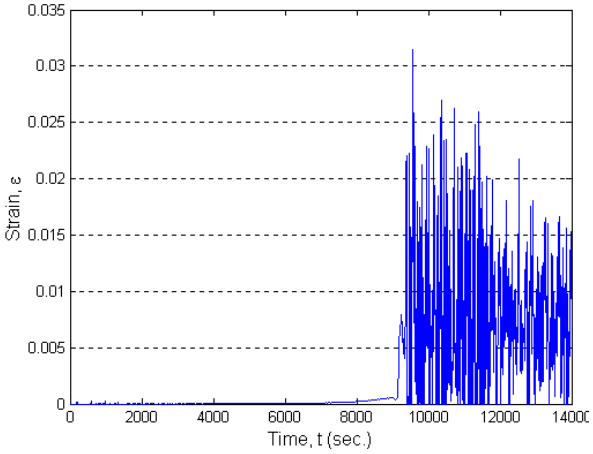

Figure 9: Strain in the tether element connected to the probe.

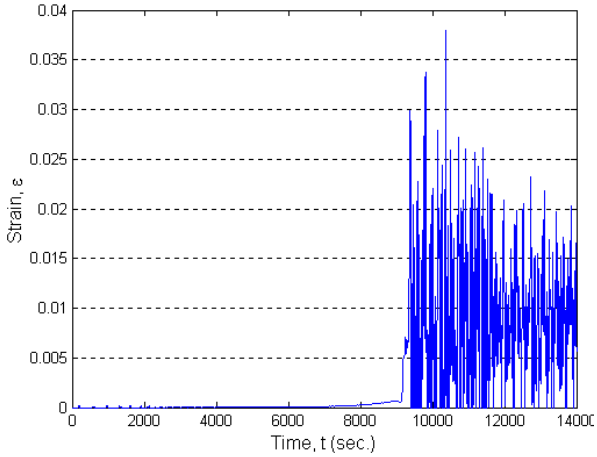

Figure 10: Strain in the tether element connected to the orbiter.

The strain histories represented in Figs. 9 and 10 depict responses that are beyond the capabilities of the

material implemented in the simulation. In the link connected to the orbiter and the link connected to the probe, the strain exceeds the 3% limit of the Spectra material. Correspondingly, the stresses in these links exceed the tensile strength of the material. In both links, the strain becomes negative, indicating that the tether becomes slack. This is a highly undesirable situation, which is ignored by the algorithm as all negative strains are set to zero.

CONCLUSIONS

The ability of a dissipative time-stepping algorithm derived from finite element theory is shown to be capable of simulating the three dimensional behavior of an elastic tethered system. A representative simulation is completed over an elliptic orbit corresponding to several hours flight time and considers the effect of atmospheric breaking and a non-spherical gravitational potential field. The strain history profiles clearly indicate the need to include suitable control techniques. With appropriate validation and refinement, the modeling technique presented here will become a valuable and flexible simulation tool.

ACKNOWLEDGEMENTS

This work was made possible, in part, through the Graduate School Research Travel Award (GSRTA) scheme of the University of Queensland Graduate School.

REFERENCES

[1]Kuhl, D. and Crisfield, M., "Energy-conserving and decaying algorithms in nonlinear structural dynamics", *International Journal for Numerical Methods in Engineering,* Vol. 45, 1999, pp. 569-599.

[2]Daniel, W. J. T., "Explicit/Implicit Partitioning of the Generalized Alpha Method," in *First Asian-Pacific Congress on Computaional Mechanics,* Sydney, Australia, 2001.

[3]Bauchau, O. A., Bottasso, C. L. and Trainelli, L., "Robust Integration Schemes for Flexible Multibody Systems," *NATO-ARW on Computational Aspects of Nonlinear Structural Systems with Large Rigid Body Motion,* edited by J. Ambrosio and M. Kleiber, Pultusk, Poland, 2000.

[4]Armero, F. and Romero, I., "On the Formulation of High-Frequency Dissipative Time-Stepping Algorithms for Nonlinear *Dynamics*. Part II: Second-Order Methods." Report UCB/SEMM-99/06, UC Berkley, 1999.

[5]Brown, K. G., Melfi, L.T. Jr., Upchurch, B.T. and Wood, G.M., "Downward-Deployed Tethered Satellite Systems, Measurement Techniques, and Instrumentation: A Review.," *Journal of Spacecraft and Rockets,* Vol. 29, No. 5**,** 1992, pp. 671-677.

[6]Wood, G. M., Siemers, P. M., Squires, R. K., Wolf, H., Carlomango, G. M. and de Luca, L., "Downward-Deployed Tethered Platforms for High Enthalpy Aerothermodynamic Research," *Journal of Spacecraft and Rockets,* Vol. 27, No. 2**,** 1990, pp. 216-221.

[7]Anderson, J. L., "Tethered Aerothermodynamic Research for Hypersonic Waveriders," *1st International Hypersonic Waverider Symposium,* NASA/University of Maryland, University of Maryland, Maryland, 1990.

[8]Bogar, T. J., Bangham, M. E., Forward, R. L., Lewis, M. J., "Hypersonic Airplane Space Tether Orbital Launch (HASTOL) System: Interim Study Results," *9th International Space Planes and Hypersonic Systems and* Technologies *Conference,* AIAA Paper 99-4802, AIAA, Norfolk, VA, 1999.

[9]Pasca, M. and Lorenzini, E., "Collection of Martian Atmospheric Dust with a Low Altitude Tethered Probe," *Advances in the Astronautical Sciences,* Vol. 75, 1991, pp. 1121-1139.

[10]Pasca, M. and Lorenzini E. C., "Optimization of a Low Altitude Tethered Probe for Martian Atmospheric Dust Collection," *Journal of the Astronautical Sciences*, Vol. 44, 1996, pp. 191-205.

[11]No, T. S. and Cochran, J. E., Jr., "Dynamics and Control of a Tethered Flight Vehicle," *Astrodynamics,* Vol. 76, 1991, p. 2429.

[12]No, T. S. and Cochran, J. E., Jr., "Dynamics and Control of a Tethered Flight Vehicle," *Journal of Guidance, Control, and Dynamics,* Vol. 18, 1995, pp. 66-72.

[13]Bae, G., Sim, E. and Barlow J. B., "Atmospheric Flight Equations of a Tethered Hypersonic Waverider," *Advances in the Astronautical Sciences,* Vol. 82, 1993, pp. 1283-1296.

[14]Santangelo A. D. and Johnson G. E., "Optimal Wing Configuration of a Tethered Satellite System in Free Molecular *Flow*," *Journal of Spacecraft and Rockets,* Vol. 29, 1992, pp. 668-670.

[15]Warnock, T. W. and Cochran, J. E., Jr., "Predicting the Orbital Lifetime of Tethered Satellite Systems," *Acta Astronautica,* Vol. 35, No. 2-3**,** 1995, pp. 193-203.

[16]Longuski, J. M. and Puig-Suari, J., "Hyperbolic Aerocapture *and* Elliptic Orbit Transfer with Tethers," *Forty-Second International Astronautical Federation Congress,* IAF Paper 91-339, Montreal, Canada, 1991.

[17]Longuski, J. M., Puig-Suari, L. J. and Mechalas, J., "Aerobraking Tethers for the Exploration of the Solar System," *Acta-Astronautica,* Vol. 35, No. 2-3**,** 1995, pp. 205-214.

[18]Tragesser, S. G., Longuski, J. M. and Puig-Suari, J., "Global Minimum Mass for Aerobraking Tethers," *Journal of Guidance, Control, and Dynamics,* Vol. 20, No. 6**,** 1997, pp. 1260-2.

[19]Biswell, B. L., *Active control of an atmospheric tether using a lifting probe*, Ph.D. thesis, Department of Mechanical and Aerospace Engineering, Arizona-State-University, Tempe, AZ, 1998.

[20]Jokic, M. D., Asokanthan, S. F., Daniel, W. J. T. and Mee, D. J., "AeroGravity Assist Manoeuvring of a Tethered Satellite System," *AIAA Atmospheric Flight Mechanics Conference,* AIAA Paper 2001-4071, Montreal, Quebec, 2001.

[21]Gonzalez, O. and Simo, J.C., "On the Stability of Symplectic and Energy-Momentum Algorithms for nonlinear Hamiltonian Systems with Symmetry," *Computer Methods in Applied Mechanics and Engineering*, Vol. 134, No. 3 and 4, 1996, p 197.

[22]Chung, J. and Hulbert, G. M., "A Time Integration Method for Structural Dynamics with Improved Numerical Dissipation: the Generalized-alpha Method," *Journal of Applied Mechanics*, Vol. 60, 1993, pp. 371-375.

[23]Prussing, J. E. and Conway, B. A., *Orbital Mechanics*, Oxford University Press, New York, 1993.